Wear 304 (2013) 49–59

Contents lists available at SciVerse ScienceDirect

Wear

journal homepage: www.elsevier.com/locate/wear

Assessing the influence of shear stress and particle impingement on inhibitor efficiency through the application of in-situ electrochemistry in a CO_2-saturated environment

O.O. Ige [a,b,*], R. Barker [a], X. Hu [a], L.E. Umoru [b], A. Neville [a]

[a] Institute of Engineering Thermofluids, Surfaces and Interfaces, School of Mechanical Engineering, University of Leeds, Leeds LS2 9JT, United Kingdom
[b] Department of Materials Science and Engineering, Obafemi Awolowo University, Ile-Ife, Osun State 220005, Nigeria

ARTICLE INFO

Article history:
Received 28 August 2012
Received in revised form
6 April 2013
Accepted 15 April 2013
Available online 23 April 2013

Keywords:
Inhibitor
Concentration
Flow-induced corrosion
Submerged impinging jet
Carbon dioxide
Velocity

ABSTRACT

An investigation was conducted to assess the performance of a commercially available high shear carbon dioxide (CO_2) corrosion inhibitor in a series of flow-induced corrosion and erosion–corrosion environments. The purpose of the study was to understand the role that high shear stress and sand particle impingement play in influencing the in-situ corrosion rate of API 5L X65 carbon steel in blank and inhibited conditions. Tests were conducted at 45 °C in CO_2-saturated conditions using a rotating cylinder electrode (RCE) for low shear stress tests (18–260 Pa) and a submerged impinging jet (SIJ) for high shear environments (104–740 Pa). The inhibitor was studied at concentrations of 0, 25, 50, 75 and 100 ppm. The application of computational fluid dynamics to model the SIJ and the use of ring shaped samples allowed for an accurate prediction of shear stress across the specimen surface that could be correlated with in-situ corrosion rate and inhibitor efficiency over a range of concentrations. The incorporation of 500 mg/L of sand to the system helped to quantify the increase of the in-situ corrosion rate due to the impingement of the particles. All corrosion rates were determined through the application of linear polarization measurements throughout the duration of the test. Post-test analysis of the material degradation mechanisms was examined using scanning electron microscopy (SEM).

1. Introduction

Flow-induced carbon dioxide (CO_2) corrosion and erosion–corrosion, which normally results in severe pipeline degradation, are important and inevitable challenges in the oil and gas industry. Erosion–corrosion in oil and gas production tends to occur due to the presence of a corrosive CO_2 environment coupled with the presence of sand particles and hydrocarbon [1]. Numerous failures have been associated with erosion–corrosion in the oil and gas industry, with this particular form of attack contributing to 15% of the total failures [2]. The consequences of such failures result in economic loss, increased downtime and maintenance costs [3]. Erosion–corrosion damage within pipelines and associated fluid handling equipment is prevalent in the oil and gas sector, particularly on facilities where low formation strength is found in wells [4].

For oil and gas transportation pipelines, internal corrosion mitigation can be achieved by the use of chemical inhibitors, which have been found to be effective in reducing corrosion to acceptable levels. One concern operators have with corrosion inhibitors is their film efficiency when subjected to high velocity and high shear stress environments. Inhibitor efficiency may be affected through lack of film formation due to high shear forces or destruction of pre-formed protective films [5]. Effective chemical inhibition of steel in CO_2 environments under high shear has long been a challenge, particularly if sand is also present in the system. It was believed that if inhibitors adsorb on the metal (or corrosion product) surface the resulting corrosion rate would only be dependent on concentration and not on flow rate [6]. Furthermore, there is a general belief that above a certain critical fluid velocity, corrosion inhibition would no longer be possible. Systematic research efforts have shown that corrosion inhibition is possible at higher flow rates for certain types of inhibitors, but at the cost of significantly higher concentrations [6]. In multiphase systems experiencing high velocity there is a need for high shear corrosion inhibitors to prevent corrosion [7]. Many studies have established the effectiveness of high shear resistant inhibitors in providing protection under erosion–corrosion environments as well as in areas of high turbulent [8–13]. A study examined the performance of a high shear corrosion inhibitor in CO_2 and CO_2/H_2S environments with and without sand [14]. It was concluded that the

(*) Corresponding author at: Obafemi Awolowo University, Department of retain->Materials Science and Engineering, Along Ife-Ibadan Expressway, Ile-Ife, Osun, Nigeria. Tel./fax: +234 8083987536.
E-mail address: ige4usa@yahoo.com (O.O. Ige).

0043-1648
http://dx.doi.org/10.1016/j.wear.2013.04.013

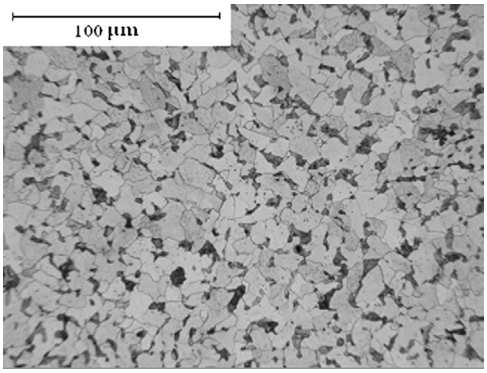

Fig. 1. Optical microscope image of X 65 carbon steel parent metal after being polished and etched in 2% nital solution for 10 s indicating regions of pearlite and ferrite.

product used in their study is suitable for deepwater and on-shore applications. Also the product exhibits better water quality attributes than other high shear corrosion inhibitors that work in CO_2 environment in the presence of sand [7].

One way to estimate pipeline degradation rates in the field is to determine the hydrodynamic parameters on the field and conduct laboratory corrosion tests accordingly to simulate the hydrodynamic parameters as closely as possible. The fundamental assumption in this approach is that, when the hydrodynamic parameters in two different geometries are the same, then the corrosion rates are the same and hence the inhibitor performances are similar [15]. The two geometry independent parameters used to describe the flow conditions in a pipe are wall shear stress and mass transfer coefficient.

Several researchers have used the jet impingement technique to study erosion–corrosion in the laboratories [9,16–18]. It has been shown that corrosion rates obtained using the jet impingement method have good correlation to pipe flow and the operating systems based on wall shear stress for $r/r_o=3$, where r is the radial distance from the centerline of the pipe and r_o is the pipe radius [19]. The flow pattern at the impinged surface has been extensively studied and several detailed mathematical expressions of the hydrodynamics are available.

These have mainly focused on the stagnation and the transition region [20–22]. It has been found that a relationship exists between fluid flow (flow rate, turbulence) and corrosion [23]. It is for this reason that corrosion models have been developed over the years with attempt to establish the relationship between fluid dynamics, mass transport and ultimately the chemical and electrochemical reactions rates occurring on the surface of metal [6]. CFD is one of the numerous tools used by researchers to investigate flow assisted corrosion and erosion–corrosion [24]. Experimental investigation of flow assisted corrosion behavior of X65 pipeline steel was carried out in the CO_2-saturated formation water by electrochemical measurements using an impingement jet system. The flow field distribution on the electrode surface was determined by computational fluid dynamics (CFD) simulation. The role of fluid hydrodynamics in FAC of the steel was mechanistically determined and also the effect of impact angle on corrosion of the steel is attributed to the distribution of fluid flow field and shear stress on the electrode surface [25].

In this study, computational fluid dynamics (CFD) is used along with a rotating cylinder electrode (RCE) and a submerged impinging jet (SIJ) to enable a correlation to be established between shear stress and corrosion rate/inhibitor efficiency over a range of inhibitor concentrations from 0 to 100 ppm. The study focuses primarily on the in-situ corrosion rate in both environments. Whilst there is a large volume of literature on the use of CFD to predict materials selection, material degradation mechanisms, and sand concentration on the flow assisted corrosion [6,26,27]; little attention has been paid on the effect of shear stress on an inhibited and uninhibited solution in the wall jet hydrodynamic zone. The goals of the study presented below are to investigate the influence of shear stress on the efficiency of a high shear CO_2 corrosion inhibitor by electrochemical techniques.

The effects of sand loading and particle impingement on in-situ corrosion rate are also determined in both environments for a concentration of 500 mg/L. The in-situ corrosion rate is the corrosion rate, measured electrochemically, when there is impingement by liquid or a liquid–solid stream at the surface. It therefore includes a measurement of the erosion or fluid enhanced corrosion term. Also, investigated are the additional effects of increased mass transfer and the effect of physical damage by sand impact on the surface [9]. The research presented in this paper focuses purely on the in-situ corrosion rate and the influence of shear stress and particle impingement on this particular component of material loss in the system. The total degradation rates in the system (i.e. the contribution of pure erosion and the effect of corrosion on erosion) are not considered here.

2. Experimental procedure

2.1. Materials

The material used in this study is API 5L X65 carbon steel with Vickers hardness of 228HV. The microstructure revealed a typical hypo eutectoid steel having less than 0.8% carbon content. The steel consists of a ferrite–pearlite microstructure as shown in Fig. 1. The chemical composition is as listed in Table 1.

The RCE samples were cylindrically shaped (12 mm diameter, 8.1 mm height and 3.13 cm^2 area).

The geometry of the samples chosen for the SIJ test was annular rings with external and internal diameters of 25 mm and 15 mm, respectively. The explanation for the choice in geometry will be provided later.

Prior to every test the specimens were polished with 1200 silicon carbide paper, degreased in acetone, rinsed with distilled water and dried with compressed air.

2.2. Brine preparation

Brine composition for the study is provided in Table 2 according to the work of Hu et al. [28]. Prior to starting every experiment, the brine solution was sparged with CO_2 for a minimum of 12 h to achieve an oxygen concentration of below 20 ppb to simulate the field conditions. The vessels were sealed in every test and CO_2 was bubbled into the system throughout the experiment to maintain CO_2 partial pressure at 1 bar.

Table 1
Nominal compositions of API 5L X65 carbon steel (wt%).

Elements	Mass %
Carbon	0.10
Silicon	0.18
Manganese	1.21
Phosphorus	0.009
Sulfur	0.003
Chromium	0.10
Molybdenum	0.16
Nickel	0.07
Titanium	<0.01
Iron	Balance

Table 2
Composition of brine used in flow-induced corrosion and erosion–corrosion tests.

Preparation	(mg/L)
NaCl (sodium chloride)	24,090
KCl (potassium chloride)	706
$CaCl_2 \cdot 2H_2O$ (calcium chloride di-hydrate)	1387
$MgCl_2$ (magnesium chloride)	4360
$BaCl_2 \cdot 2H_2O$ (barium chloride di-hydrate)	16
$SrCl_2 \cdot 6H_2O$ (strontium chloride hexa-hydrate)	33
Na_2SO_4 (sodium sulfate)	3522
$NaHCO_3$ (sodium bicarbonate)	304

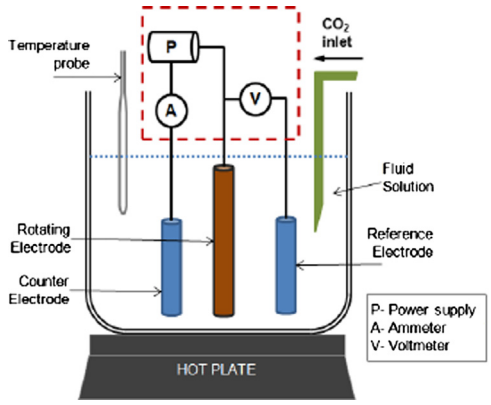

Fig. 2. The setup of the rotating cylinder electrode (RCE).

2.3. Inhibitors

A commercially available, high shear CO_2 inhibitor was used in the test presented and is referred to as Inhibitor A. The chemical package is based on a combination of anhydrides, polyamines, ethoxylated imidazolines, quaternary ammonium salts, ethanodiol and thioalcohol. Inhibitor A was tested at concentrations of 0, 25, 50, 75, and 100 ppm.

The inhibition efficiency was calculated using Eq. (1) which is based purely on the reduction of the in-situ corrosion rate from electrochemical measurements over the test duration [28], such that

$$\text{Inhibition efficiency} = [(CR_{NI} - CR_{WI})/CR_{NI}]100 \quad (1)$$

where, CR_{WI} and CR_{NI} are the in-situ corrosion rates with and without inhibition respectively.

2.4. Flow-induced corrosion and erosion–corrosion setup

The flow-induced corrosion and erosion–corrosion experiments were conducted using a rotating cylinder electrode (RCE) and a submerged impingement jet (SIJ) apparatus as shown in Figs. 2 and 3, respectively. The two sets of apparatus were used in order to achieve a wide range of shear stress values and flow velocities.

RCE tests were conducted at rotational speeds of 1000, 3000 and 5000 rpm. The RCE working electrodes were held between polytetrafluoroethylene (PTFE) washers and mounted on the rotating disk. The electrochemical measurements were conducted as reported by Wang et al. [10]. The corrosion rate for the SIJ was determined by using the linear polarization resistance (LPR) technique according to the work of Xu and Neville [27]. retain–>A recirculating system is adopted by the rig which delivers the process fluid (with or without sand) through two nozzles which impinge onto flat specimens at an angle of 90°. The both nozzles have a diameter of 4 mm with the standoff distance being kept constant at 5 mm. Velocities chosen for the tests were 5, 10, and 15 m/s.

Tests were conducted without solid loading for flow-induced corrosion and with the addition of 500 mg/L of sand to create an erosion–corrosion environment. Round silicon sand particles which are un-ground were used in these studies with an average diameter of 250 μm. The shape and size distribution are as illustrated in Fig. 4(a) and (b). All experiments were conducted for 4 h at a temperature of 50 °C.

2.5. Surface analysis

The post-test analysis of the material damage mechanisms was examined by a scanning electron microscope (SEM). The analysis revealed the extent and nature of mechanical and electrochemical damage in the absence and presence of inhibitors. Also, the effects of loading with or without solid particles were observed.

2.6. Computational fluid dynamic (CFD) modeling

The shear stress over the surface of RCE samples has been well characterized [19,26,30,31]. However, the hydrodynamic conditions over SIJ specimens in the wall jet region have received less attention. Therefore, CFD modeling of the SIJ was adopted to determine the shear stress distribution over the sample surface.

The model for the SIJ is assumed to be axisymmetric about the centerline of the pipework. A 2D model was implemented; hence, the resulting flow domain on any particular plane along this centerline and perpendicular to the test surface is expected to be representative of the entire flow domain. Adopting this technique helped to minimize computing resources without compromising solution accuracy. The computational domain consisted of over 130,000 triangular elements and the fluid was treated as viscous, turbulent, incompressible and isothermal. A larger number of cells were used to resolve the region closer to the sample surface. The computational mesh was refined to ensure that the boundary layer was adequately resolved and grid independence obtained. An inflow condition at the SIJ nozzle inlet was used where the mean velocity of flow was specified. The k–ε model was chosen to numerically simulate the effects of turbulence over the jet. All numerical simulations were solved using the second order upwind interpolation scheme. The simple algorithm was also employed to guarantee a cross linkage between the pressure and velocity, which predominantly accounts for the mass conservation within the flow domain. All numerical simulations were converged when the residuals of all flow parameters fell below 1×10^{-5}. An image of the velocity flow field is provided in Fig. 4(a) for flow at 5 m/s as an example. Modeling the flow from the SIJ allows the wall shear stress on the surface of the specimen to be determined (Fig. 4(b)). The distributions indicated that the shear stress across the surface is relatively constant at a radial distance of between 7.5 and 12.5 mm from the center of the sample. This is the reason why ring samples were manufactured, as this helped to ensure a stable shear stress was applied to the surface in the SIJ, just as in the RCE.

The CFD simulation was performed using the following conditions:

i. Grid resolution: 47116 elements.
ii. Criterion used to finish each calculation, 1×10^{-5}.
iii. The wall boundary condition is assigned to no flow across the surface, that is the flow velocities on all solid walls are zero due to the implementation of no slip-condition [29].
iv. Inflow conditions: 5, 7, 10, 12, and 15 m/s.
v. Outflow condition: atmospheric pressure (101.325 kPa).
vi. Turbulent κ–ε and dissipation: RNG κ–ε.

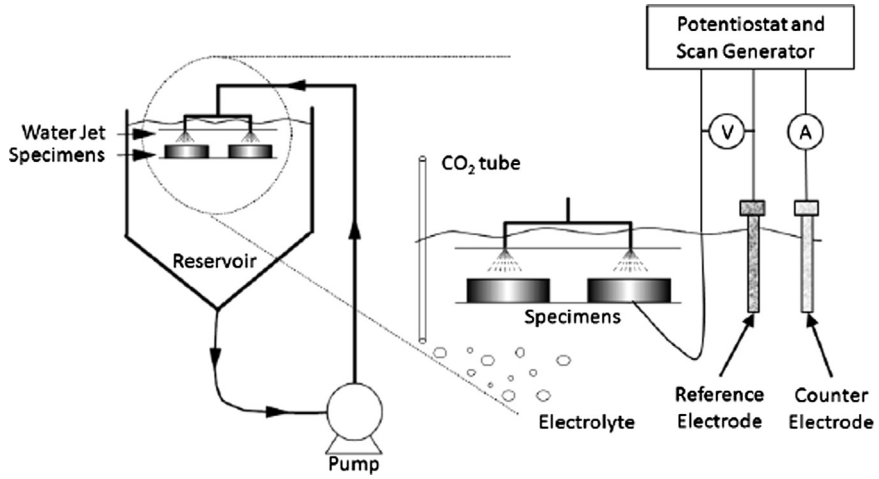

Fig. 3. Re-circulation rig for CO_2 erosion–corrosion experiments.

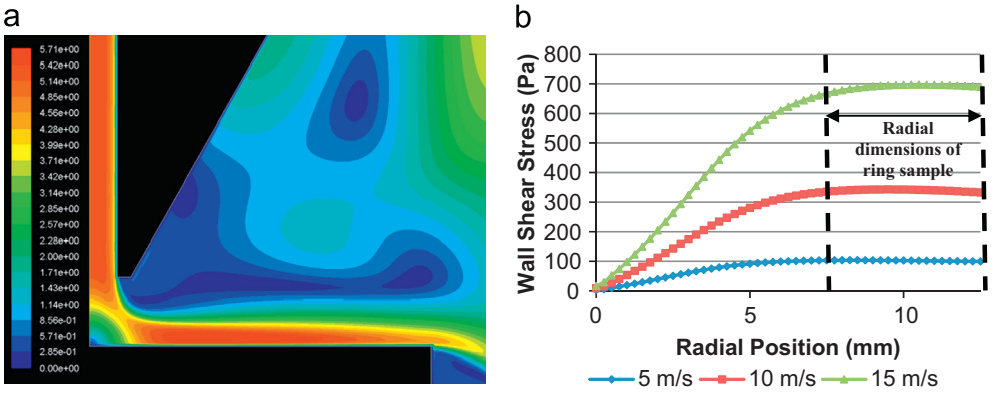

Fig. 4. (a) Velocity contours of flow from submerged impinging jet onto a sample at 90° at 5 m/s and (b) wall shear stress as a function of radial distance from the center of the carbon steel specimens extracted from the CFD model.

3. Results and discussion

3.1. Uninhibited conditions

In order to evaluate the inhibitor performance at different velocities, the corrosion rates for the API 5L X65 steel were monitored over 4 h. Fig. 5a and b shows that the in-situ corrosion rate values remain relatively constant as a function of time in both RCE and SIJ environments at various velocities without presence of corrosion inhibitor. The steady-state corrosion potential ranges between 653 and 677 mV for the SIJ conditions. The corrosion rates in the SIJ were much higher than RCE values as expected.

Corrosion rate results for tests conducted with addition of 500 mg/L sand are provided in Fig. 6(a) for the RCE and Fig. 6 (b) for the SIJ systems. It is clear that there is only a very small effect of the addition of sand on the corrosion degradation rate.

The average of the final corrosion rates over the duration of the tests are summarized in Fig. 7. The introduction of solid particles into the environment for the SIJ increased the extent of degradation at all flow velocities. However, no noticeable increase in the in-situ corrosion rate can be observed for tests in the RCE at the rotating speeds of 3000 and 5000 rpm. Whereas there is a sharp difference in the degradation rates between the flow induced corrosion and erosion–corrosion for samples subjected to rotating speed of 1000 rpm. The shear stress is considered to be too low such that the harmful effects of mass transfer are highly negligible. With the introduction of solid particles there is an increased impingement and escalation in the adsorption–desorption cycles (exposure of the active metal) on the steel surfaces. It can also be postulated that the kinetic energy increased the adsorption–desorption cycle of the electrode thereby increasing the corrosion products removal rate from the material surface [32].

The shear stress values for the RCE were calculated by using equations derived by Silverman [31]:

$$\tau_w = 0.0791 Re^{-0.3} \rho r^2 \omega^2 \quad (2)$$

where, Re is the Reynolds number, ρ is the solution density (g cm^{-3}), ω is the rotation rate (rad/s), and r is the radius of the outer diameter (cm).

The corrosion rates of the samples as a function of wall shear stress for the flow-induced corrosion tests can be plotted as shown in Fig. 8. This result is in agreement with an earlier work as reported by Effird et al. [19]. It is clear that corrosion rate increases as a function of the flow shear stress. The ring samples subjected to SIJ exhibit a higher corrosion rate compared with the RCE at equivalent values of shear stress. This can be attributed to the difference in the behavior of the RCE and SIJ. This difference is not well understood [19]. The only explanation for the difference can be offered only on the basis of transfer phenomena that are whether the material is charge transfer controlled or is under diffusion controlled. Also shear stress has been conceived to be a geometry-independent indicator of the degree of turbulence in the flow [19]. In this study the nonlinear relationship is considered to be mild in nature [33,34]. The logarithmic relationship between the corrosion rate and the shear stress for both systems with and without sand is believed to be governed by a diffusion reaction mechanism. This mechanism is based on the case whereby the

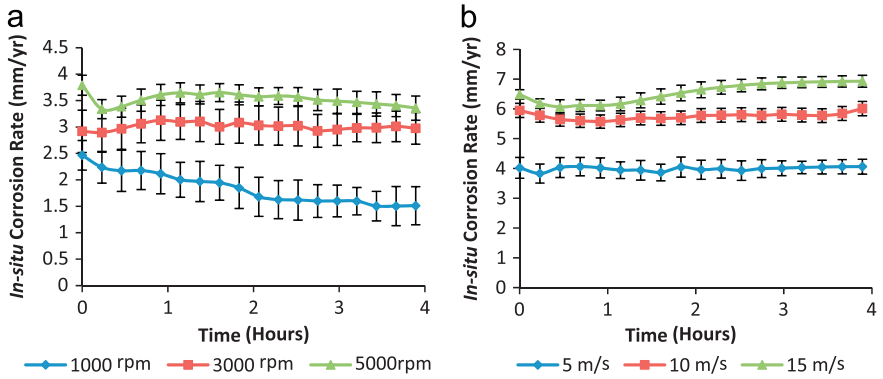

Fig. 5. In-situ corrosion rate as a function of time for API 5L X65 at different (a) rotational speeds in RCE and (b) impingement velocities in SIJ for a blank flow-induced corrosion environment.

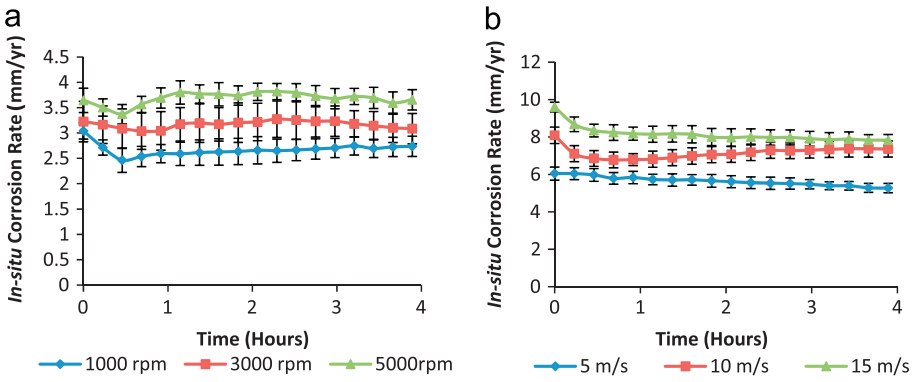

Fig. 6. In-situ corrosion rate as a function of time for API 5L X65 at different (a) rotational speeds in RCE and (b) impingement velocities in SIJ for a blank erosion–corrosion environment with 500 mg/L sand.

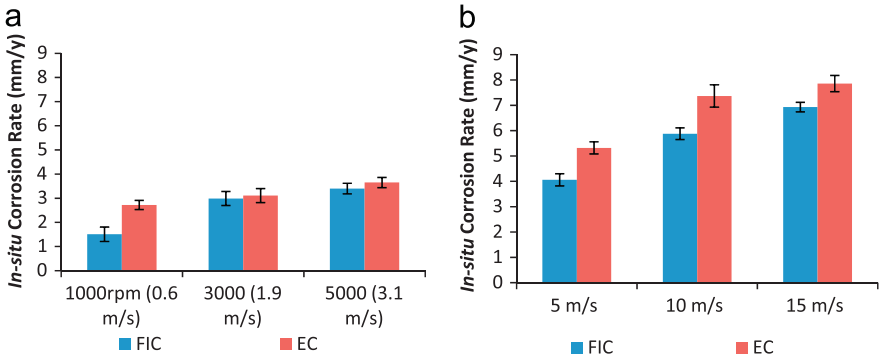

Fig. 7. The in-situ corrosion rates for flow-induced corrosion and erosion–corrosion tests in blank conditions for (a) RCE and (b) SIJ.

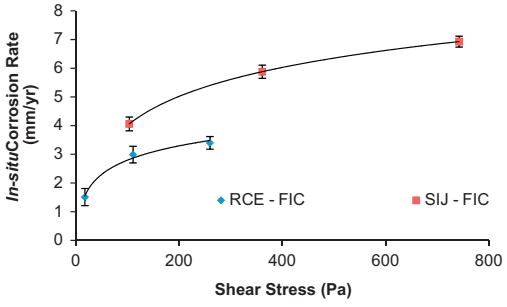

Fig. 8. In-situ corrosion rate as a function of wall shear stress in blank flow-induced corrosion tests with the RCE and SIJ.

reactants influence the chemical reactions in which the electrode–electrolyte is transferred into each other, and the diffusion which causes the reacting species and corroded products to spread out. The addition of solid particles will enhance the cutting mechanism on the steel surface [35,36]. It will also increase the movement of the reacting species to the steel substrate and the removal of the corroded products from the steel surface.

3.2. Inhibited conditions

All the tests performed in blank conditions were repeated with the addition of 25, 50, 75 and 100 ppm Inhibitor A. The steel samples were immersed into the inhibited process fluid after the inhibited solution must have achieved a steady-state potential. Typical corrosion rate behavior as a function of time is provided in Fig. 9(a) for the RCE and Fig. 9(b) for the SIJ at a concentration of 100 ppm Inhibitor A. The results indicate the immediate effect in reducing the corrosion rate as inhibitor is introduced into the system.

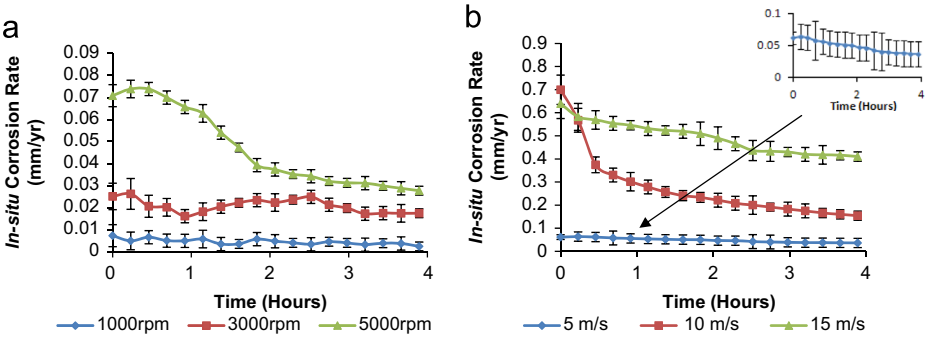

Fig. 9. In-situ corrosion rate as a function of time for API 5L X65 at different (a) rotational speeds in RCE and (b) impingement velocities in SIJ for a blank erosion–corrosion environment with 500 mg/L sand.

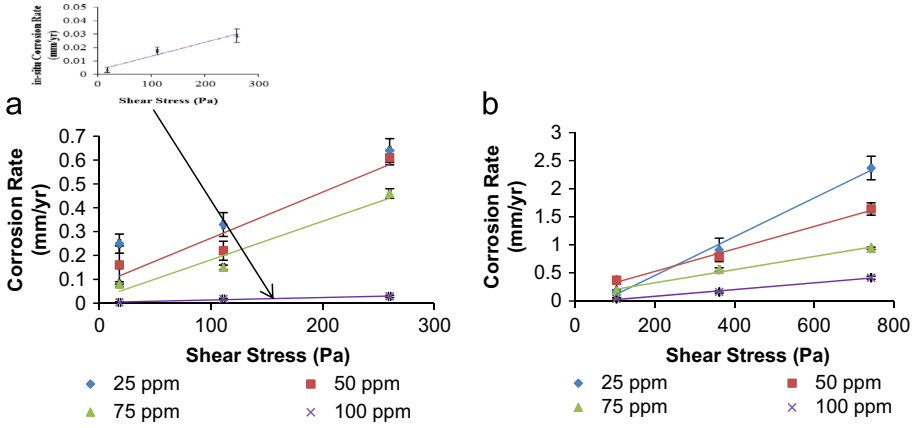

Fig. 10. In-situ corrosion rate as a function of wall shear stress for X-65 in (a) the RCE and (b) in the SIJ for flow-induced corrosion experiments.

Fig. 10 compares the RCE and SIJ results for the inhibited system at various shear stresses at various corrosion inhibitor concentrations. There is a linear relationship between the shear stress and corrosion rate. This is in contrast to the results as obtained for the uninhibited system and Effird et al.'s study in blank solution which reported that the corrosion rate increases with shear stress as a power function with linear relationship on a full logarithm scale [19]. The linear relationship indicates that the reaction rates and equilibriums greatly influenced the corrosion reactions. This implies that the presence of inhibitors will promote the formation of corrosion products and boost the adsorption of the inhibitor constituents on the steel surface. It has been reported the limiting current for H_2CO_3 have two components, namely; a flow-independent part – chemical reaction controlled, and a flow-dependent part – mass transfer controlled. The blank solution is governed by the latter part while the inhibited environment is controlled by the chemical reaction. It must also be noted that the inhibitor is an imidazoline based chemical package which is a family of organic inhibitor. Hence the inhibitor is an adsorption type and the limiting current will be determined by the surface chemistry reactions [37].

3.3. *Inhibitor efficiency in the RCE*

The inhibition efficiencies (IE) of the RCE system are as presented in Fig. 11. There is an increase in the efficiency as the concentration of the inhibitor increases while there is a very slight decrease as the shear stress increases. The acceleration of corrosion under flowing conditions has been ascribed to either mechanical removal of corrosion products from the metal surfaces or to mass transfer effects or both [38].

The introduction of solid particles increases the rate of degradation both for uninhibited and inhibited samples. Hence the addition of sand significantly reduces performance and reduction in performance is more significant at 3000 and 5000 rpm than at 1000 rpm. There is a large difference between the inhibition efficiencies at 1000 and 3000/5000 rpm when sand is present for the system inhibited with 25–75 ppm concentration. The introduction of 100 ppm inhibitor significantly reduces the efficiency between 1000 and 3000 rpm transition. The inhibitor is regarded to be responsible for the reduction in the mechanical damage caused by sand and this is an additional effect not often realised in inhibited systems [10]. The anodic electrochemical reactions for low carbon steel corrosion in CO_2—containing shows that iron dissolution is predominant and it is according to the following equation [39]:

$$Fe = Fe^{2+} + 2e^{-} \quad (3)$$

It is believed that the metal corrosion is suppressed by the inhibitors. The inhibitors being organic are regarded as adsorption or film forming inhibitors on metal surface even at high shear stress multiphase system and in the presence of sand particles [10,40].

With the introduction of an organic inhibitor, the first step during the adsorption of an organic inhibitor on a metal surface is usually regarded as replacement of water molecules absorbed on the metal surface [41].

$$Inh_{sol} + xH_2O = Inh_{ads} + xH_2O_{sol} \quad (4)$$

The adsorbed inhibitor will combine with freshly generated Fe^{2+} ions on the steel surface to form metal inhibitor

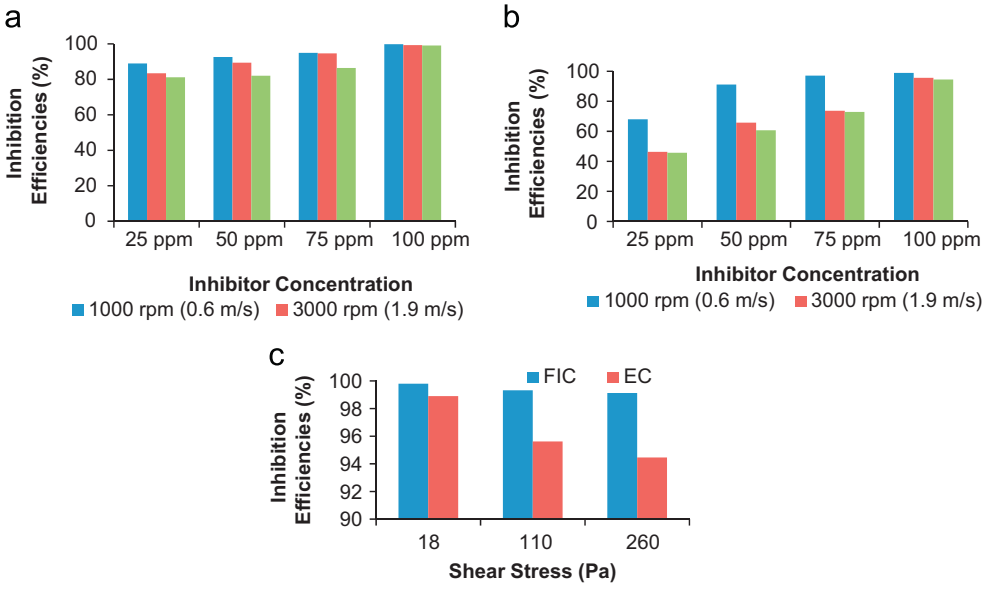

Fig. 11. The inhibition efficiency of RCE at various inhibition concentrations: (a) FIC, (b) EC, (c) comparison of FIC and EC with 100 ppm inhibitor.

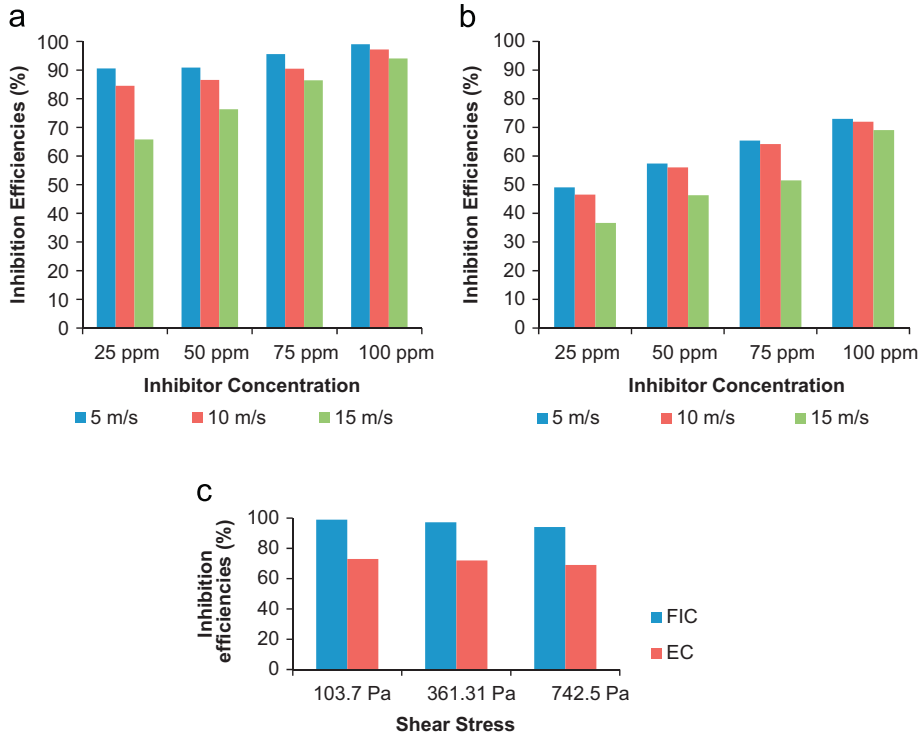

Fig. 12. The inhibition efficiency of SIJ at various inhibition concentrations: (a) FIC, (b) EC and (c) comparison of FIC and EC with 100 ppm inhibitor.

complexes [42, 43]

$$Fe = Fe^{2+} + 2e^{-} \quad (5)$$

$$Fe^{2+} + Inh_{ads} = Fe\text{–}Inh^{2+}_{ads} \quad (6)$$

The resulting complex, depending on its relative solubility, can either inhibit or catalyze further metal dissolution.

The effect of sand on the inhibitor efficiency is clearly shown in Fig. 11c. Obviously the efficiency decreases as the shear stress increases and it is more noticeable in the presence of sand. Based on the international practice the inhibitor is recommended for FIC and EC at inhibitor concentration of 100 ppm because the efficiency is above 90% for all the shear stresses under investigation. The maximum efficiency reduction is about 5% at 5000 rpm (260 Pa). The inhibition mechanism is to affects the impact dynamics. It has been reported that inhibitor can reduce the impact energy on the metal surface by either adsorbing on the metal surface or as well adsorb onto the sand [44] .

3.4. *Efficiency of inhibitor in SIJ*

The inhibition efficiency as a function of inhibitor concentration for SIJ is given in Fig. 12. Calculation shows that the surface shear stress increased markedly as the flow velocity is increased in this system. The surface shear stress is regarded to be directly proportional to the flow velocity [45]. The surface shear stress also

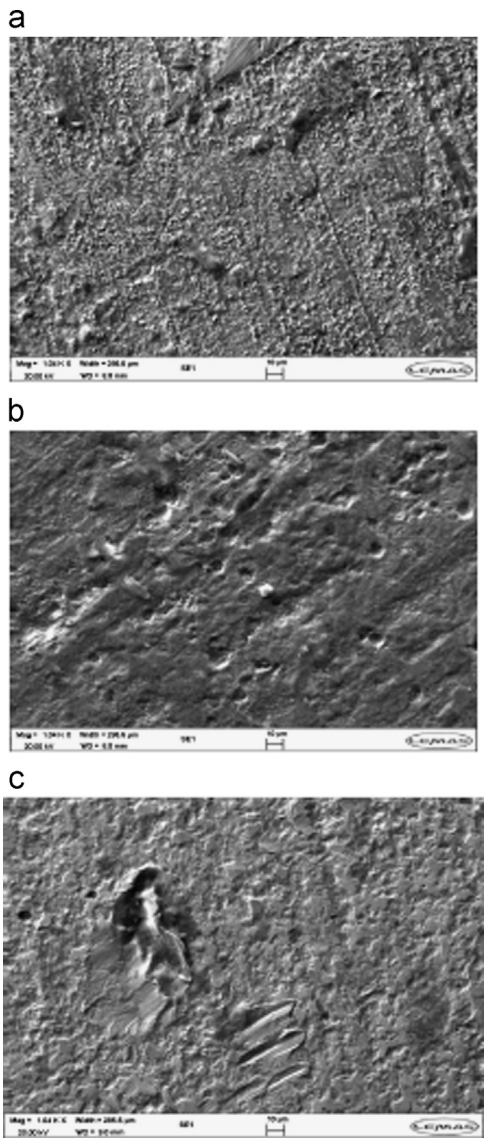

Fig. 13. SEM micrograph of erosion corrosion samples at 50 °C and different velocities: (a) 1000 rpm, (b) 3000 rpm and (c) 5000 rpm.

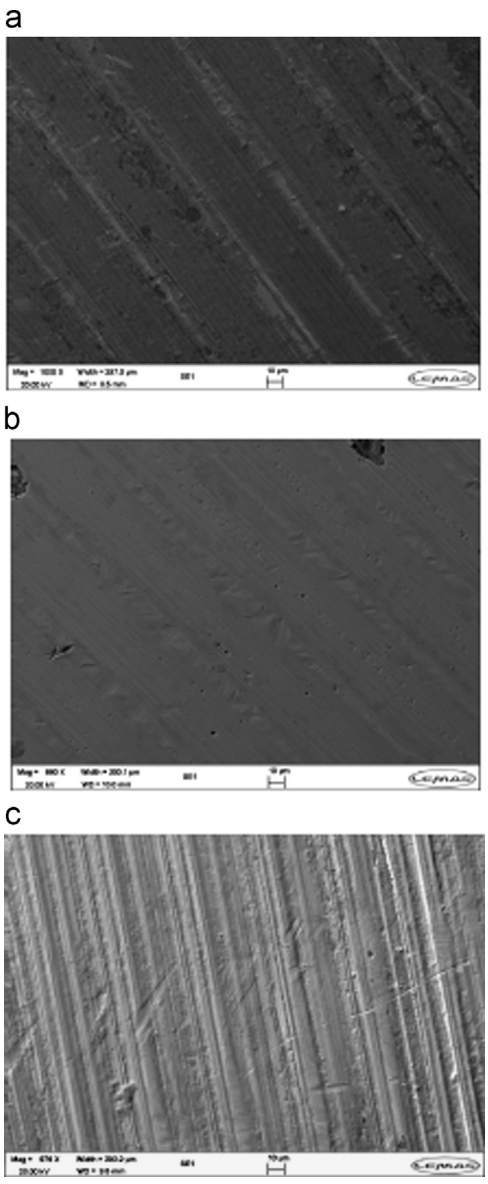

Fig. 14. SEM micrograph of erosion corrosion samples inhibited with 100 ppm at 50 °C and different velocities: (a) 1000 rpm, (b) 3000 rpm and (c) 5000 rpm.

leads to continuous removal of corrosion product, thereby exposing fresh surface matrix to the environment and ultimately aggravates the degradation mechanism. Invariably high fluid velocity will increase the surface shear stress and then the corrosion rate. This may be due to longitudinal impact motion energy which is as a result of surface pressure stress on the corrosion scale and this made cracks appeared in the corrosion scale [45]. Furthermore the data show that high frequency impact of sand particles occur, which increases the material degradation rate. The material removal mechanisms are different for both SIJ and RCE systems based on factors such as the geometry, flow velocity, impingement angles among others. This implies that there will be reduction in the in-situ corrosion rate for RCE when compared with that of SIJ.

Also, there is a drop in efficiency between 10 and 15 m/s and is largely removed by increasing the inhibitor concentration from 75 to 100 ppm. This is also in agreement with a previous study [10]. It is assumed that this will also reduce the local turbulent intensity and thereby reduce the erosion component of damage [10]. Similarly, the introduction of sand into the system also reduces the inhibition efficiency as obtained in the RCE. There is a reduction in the IE (%) as shown in Fig. 12b. However the reduction is more significant for SIJ but there is no pronounced reduction in the efficiency as the shear stress increases. This was made obvious by comparing the flow-induced corrosion and erosion–corrosion at inhibitor concentration of 100 ppm (Fig. 12c). The efficiency reduction is about 20% at all shear stress levels. For example, the efficiency of samples subjected to FIC at 10 m/s is around 90% whereas it is about 65% for EC samples.

Obviously, the additions of sand have harmful effect on the inhibitor efficiency which concur with Neville and Wang [10,44] study that stated that sand reduces inhibitor efficiency. In another of their work, they concluded that corrosion is a controlling parameter in erosion–corrosion. They also stated that corrosion aligned in the same way in erosion–corrosion for both inhibitors even though erosion is a significant part of the total damage [9]. There is a need for further work to determine whether the inhibitor adsorbed on the metal surface or on the sand.

3.5. SEM

The micrographs from SEM analysis confirm the quantitative results from in-situ corrosion measurements presented in the

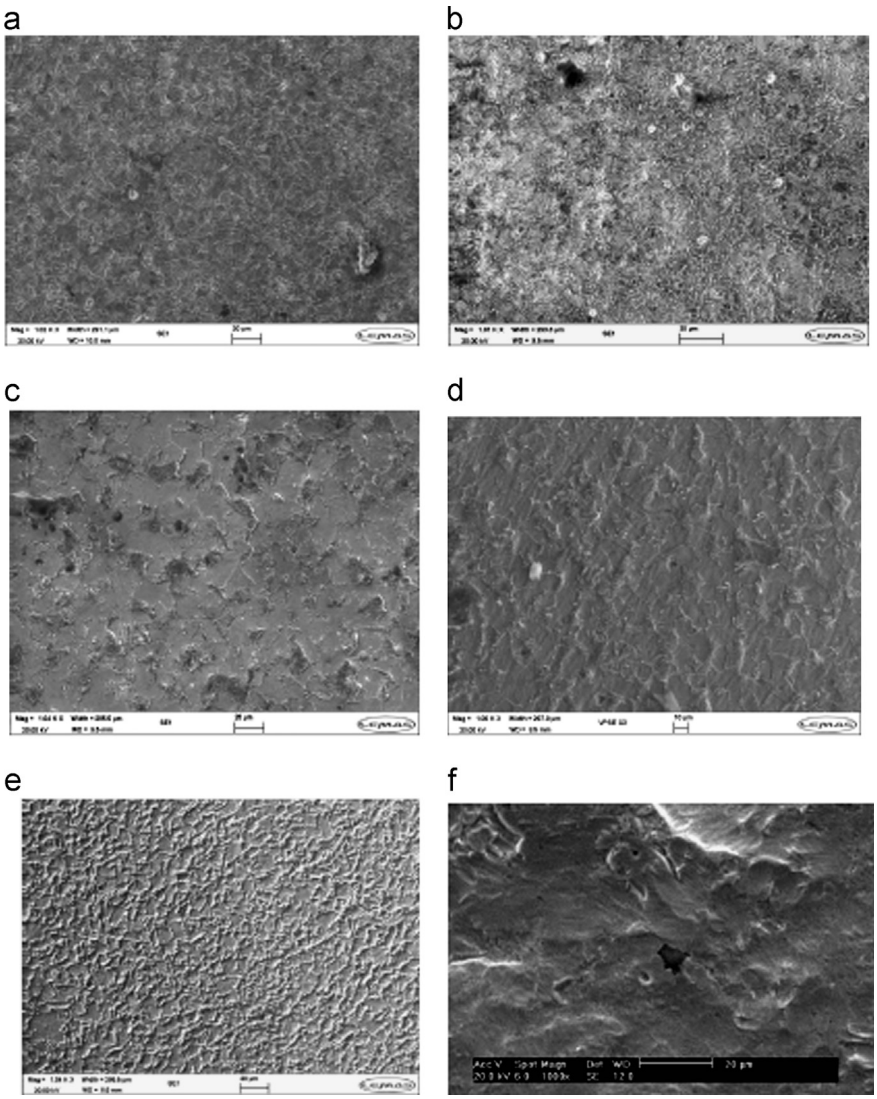

Fig. 15. SEM micrograph of uninhibited samples at 50 °C: (a) without sand at 5 m/s, (b) with sand at 5 m/s, (c) without sand at 10 m/s, (d) with sand at 10 m/s, (e) without sand at 15 m/s and (f) with sand at 15 m/s.

previous sections. Fig. 13(a–c) shows the material surfaces after exposure to the RCE system in presence of 500 mg/L sand particles at different rotating speeds. It is clear that the severity of mechanical attack increases as the flow velocity on the surface increases. There is a widespread localized attack on the substrate at 1000 rpm and there is a significant material dissolution on the steel surface (Fig. 13a). The degradation mechanism tends to be material dissolution along the flow direction. Fig. 13(b) shows that at 3000 rpm the material is subjected to plastic deformation with fewer pits distribution but of larger geometry and negligible impact scars. Material degradation occurs from massive plastic deformation and there is evidence of impact trails which exhibits a directional pattern (Fig. 13c).

The materials removal is suspected to be due to the scouring action of the sand particles. Addition of 100 ppm inhibitor shows that the material degradation is less pronounced (Fig. 14). However the mechanism of degradation is similar. Material dissolution and localized attack occurred in the low velocity regime (Fig. 14a) and at flow velocity of 3000 rpm (Fig. 14b). There is presence of plastic deformation with scattered large pits. While Fig. 14 (c) presents that at 5000 rpm there is considerable plastic deformation with insignificant material dissolution.

SEM analysis for SIJ systems was also conducted on the surfaces of ring samples for blank conditions with sand particles as presented in Fig. 15. Generally, the flow induced samples are characterized by uniform attack over the whole surface of the samples exposed. Fig. 15(a) shows pearlite regions (dark areas) and the light regions which are ferrite between the pearlite colonies. There are signs of material dissolution indicating the removal of ferrite regions had taken place. The micrograph of the erosion–corrosion sample at 5 m/s shows massive dissolution and cementite are more pronounced (Fig. 15b).

The increase in flow velocity to 10 m/s reveals that the ferrite region is widespread with scattered pearlite zones along the grain boundaries. This mismatch in grain size will further aggravate the material dissolution (Fig. 15c). The introduction of sand at this velocity reveals grain boundaries of the substrates, presence of few localized attacks with severe sizes, and plastic deformation (Fig. 15d). It is realized that as the flow velocity increases the localized attack is predominant on the grain boundaries. This corroborates the earlier trend as reported that grain boundaries have their own metallurgy which differs from that of the grains that makes them a source of corrosion initiation and propagation [29]. The increase of the flow velocity to 15 m/s shows that the ferrite regions are smaller with the pearlite segregating along the grain boundaries (Fig. 15e). The network of the pearlite–ferrite is homogeneous in size and spacing. This will further reduce the spacing between ferrite and cementite and the smaller the

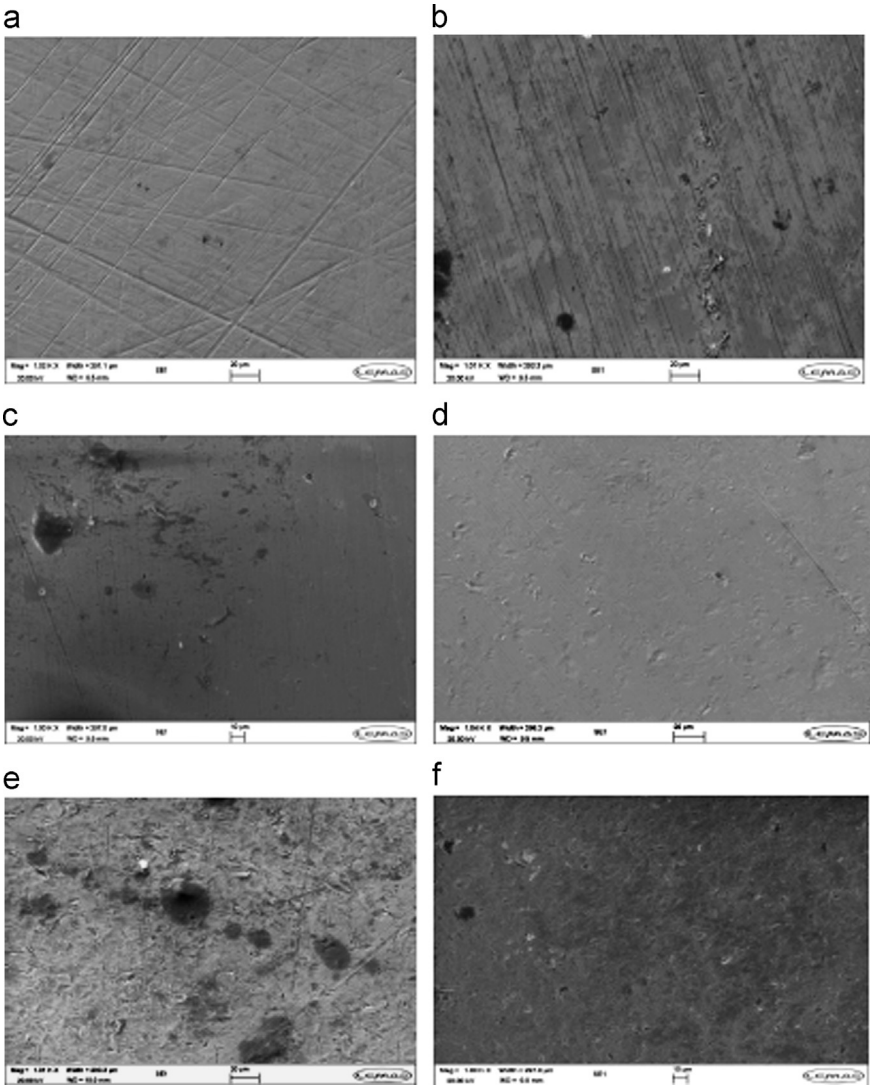

Fig. 16. SEM results for the samples inhibited by 100 ppm: (a) without sand at 5 m/s, (b) with sand at 5 m/s, (c) without sand at 10 m/s, (d) with sand at 10 m/s, (e) without sand at 15 m/s and (f) with sand at 15 m/s.

spacing, the larger the area and hence the energy of the ferrite-cementite interfaces become weaken. This will reduce the overall free energy of reaction and increase the material dissolution. As shown in Fig. 15(f), retain–>there is a huge scouring action with a heavy plastic deformation due to the particle impacts and highly localized attack resulting in perforation. There is flake generation produced from the impact scars and also material removals due to erosion cutting. On the strength of visual observation there is an increase in the total damage which may be attributed to erosion damage on the surface as a result of sand particle velocity in the flow [29].

The surface analysis of samples in the presence of 100 ppm inhibitor was as presented in Fig. 16. The inhibited samples without the presence of sand at 5 m/s have smooth surface with no sign of material loss (Fig. 16a) while the presence of sand on the images was not noticeable (Fig. 16b). This tends to show that material dissolution was dominant as against materials removal mechanism. However the introduction of solid particles slightly increases the dissolution rate as observed which corroborates the increase in corrosion rate. The increase of the flow velocity to 10 m/s for the flow-induced samples with 100 ppm of inhibitor show an increase in the rate of dissolution, and also there is presence of localized attacks (Fig. 16c). The addition of sand particles into the system characterized the images with beach marks and plastic deformation were not remarkable (Fig. 16d). The trend changed from material dissolution to removal of materials despite the presence of inhibitors at this flow velocity. This can be attributed to the influence of the shear stress and the impact energy of the sand particles. The flow-induced samples subjected to 15 m/s characterized with severe materials removal (Fig. 16e). The material degradation results from heavy plastic deformation and there is evidence of ductile tearing where lips have been formed [46]. The SEM analysis for the erosion–corrosion test in 100 ppm inhibited conditions revealed signs of significant material dissolution and relative degree of materials removal (Fig. 16f). The material dissolution shows pearlite regions protruding which indicate that the removal of ferrite regions has taken place and the materials removal were in the form of impingement marks and formation of flakes due to the sand particles.

4. Conclusions

- The rate of degradation increases as the shear stress retain–>increases for both systems (RCE and SIJ); however the

corrosion rate for SIJ is higher than that of RCE at a given shear stress level.

- The addition of sand increased the corrosion rate in SIJ but have little effects in RCE. The material degradation mechanism based on the surface roughening accounted for this and the difference in the area of geometry for the samples.
- The introduction of inhibitors decreased significantly the rate of corrosion for flow-induced and erosion–corrosion.
- The shear stresses are linearly related to the corrosion rates in the presence of inhibitor with and without sand particles. While the blank solution have a power function with linear relationship on a full logarithm scale. The relationship is affected by the transfer phenomena—mass transfer controlled or diffusion controlled.

Acknowledgments

OOI would like to thank the following organizations for their financial assistance: ETF, NIGERIA; NASENI, NIGERIA; Carnegie Corporation through OAU Linkages, NIGERIA and School of Mechanical Engineering, University of Leeds, UK.

References

[1] J.R. Shadley, S.A. Shirazi, E. Dayalan, E.F. Rybicki, Prediction of Erosion–Corrosion Penetration Rate in Carbon Dioxide Environment With Sand, NACE, 1998, San Diego, CA(Corrosion/98, Paper no. 59).
[2] M. Oberndorfer, Private Communication, OMV AG, Wien, 2003. (accessed 30.01.2003).
[3] C. Wang, A. Neville, Understanding the action of inhibitors in mitigating erosion–corrosion in impinging flows, Corrosion (2004), Paper no. 04658.
[4] A. Gnanavelu, N. Kapur, A. Neville, J.F. Flores, An integrated methodology for predicting material wear due to erosion, Wear 267 (2009) 1935–1944.
[5] Z. Tendayi, Hydrodynamics on Carbon Steel Erosion–Corrosion and Inhibitor Efficiency in Simulated Oilfields Brines, University of Glascow, Glascow, 2010.
[6] R.H. Hausler, Hydrodynamic and flow effects on corrosion inhibition, Corrosion (2004), Paper no. 04402.
[7] S. Ramachandran, V. Jovancicevic, S. Mancuso, Menedezc, Development of High Shear Corrosion Inhibitor for Mild Steel in Different CO_2 and Co_2/H_2S Environments With and Without Sand, NACE International, Houston, TX, 2011, Paper no. 11348.
[8] C. Wang, A. Neville, S. Ramachandran, V. Jovancicevic, Understanding the Action of Inhibitors in Mitigating Erosion–Corrosion in Impinging Flows, NACE International, Houston, TX, 2004, Paper no. 04658.
[9] C. Wang, A. Neville, S. Ramachandran, V. Jovancecic, Alleviation of erosion–corrosion damage by liquid–sand impact through use for chemicals, Wear 258 (2005) 649–658.
[10] A. Neville, C. Wang, Erosion–corrosion mitigation by corrosion inhibitors—an assessment of mechanisms, Wear 267 (2009) 195–203.
[11] M. Tandon, J.R. Shadley, E.F. Rybick, K.P. Roberts, S. Ramachadran, V. Jovancicevic, Flow Loop Studies of Inhibition of Erosion–Corrosion in CO_2 Environments with Sand, NACE International, Houston, TX, 2006, Paper no. 06597.
[12] S. Ramachandran, R. Peppeard, M.H. Nguyen, T. Hinojosa, Corrosion Inhibition in High Velocity Sand Containing Pipelines and its Implication on Economic Chemical Treatment, NACE International, Houston, TX, 2004, Paper no. 04660.
[13] S. Ramachandran, K.A. Batrip, C. Menendez, S. Coscio, Preventing Erosion and Erosion Corrosion Using Specialty Chemicals, SPE International Symposium on Oilfield Chemistry, Houston, TX, 2003.
[14] S. Ramachandran, V. Jovancicevic, S. Mancuso, C. Menendez, Development of High Shear Corrosion Inhibitor for Mild Steel in Different CO_2 and CO_2/H_2S Environments with and without Sand, NACE International, Houston, TX, 2011, Paper no. 11238.
[15] S. Papavinasam, A. Doiron, G. Shen, R.W. Revie, Prediction of Inhibitor Behavior in the Field from Data in the Laboratory, NACE International, Houston, TX, 2004, Paper no. 04622.
[16] A. Neville, X. Hu, M. Reyes, Corrosion and erosion corrosion behavior of a CO based alloy in Ni containing austenitic cast iron, Corrosion (2000), Paper no. 00628.
[17] A. Neville, X. Hu, Mechanical and electrochemical interactions during liquid–solid impingement on high-alloy stainless steels, Wear 251 (2001) 1284–1294.
[18] G. Schmitt, C. Werner, M. Bakalli, Fluid mechanical interactions of impingement flowing fluids with the wall-revisited with a new electrochemical tool, Corrosion (2005), Paper no. 05344.
[19] K.D. Effird, E.J. Wright, J.A. Boros, T.G. Hailey, Correlation of steel corrosion in pipe flow with jet impingement and rotating cylinder tests, Corrosion 49 (1993) 992–1003.
[20] F. Giralt, D. Trauss, Mass transfer from crystalline surfaces in an impingement jet, Part 2: erosion and diffusional transfer, Canadian Journal of Chemical Engineering 54 (1976).
[21] G. Schmitt, M. Bakalli, Measuring Techniques for Corrosion Rate Under Flow Conditions—What you Get and What you Do not Get, NACE International, Houston, TX, 2006, NACE 2006, Paper no. 06-593.
[22] Y. Chen, H. Chen, W.P. Jepson, Effects of Multiphase Flow on Corrosion Inhibitor, CORROSION/99, NACE International, Houston, TX, 1999, Paper 12.
[23] K.J. Kennelley, R.H. Hausler, D.C. Silverman, Flow Induced Corrosion: Fundamental Studies and Industry Experience, CORROSION/90, Symposium on Flow Induced Corrosion, NACE, 1991.
[24] A. Keating, S. Nesic, Numerical prediction of erosion–corrosion in bends, Corrosion 57 (7) (2001) 621–633.
[25] G.A. Zhang, Y.F. Cheng, Electrochemical characterization and computational fluid dynamics simulation of flow-assisted corrosion, Corrosion Science 52 (2010) 2716–2724.
[26] M.J. Willis, T.N. Croft, M. Coss, Computational Fluid Dynamics Modelling of an Erosion–Corrosion Test Method, NACE International, Houston, TX, 2009. (CORROSION/2009, Paper no. 09473).
[27] A. Gnanavelu, N. Kapur, A. Neville, J.F. Flores, N. Ghorbani, A numerical investigation of a geometry independent integrated method to predict erosion rates in slurry erosion, Wear 271 (2011) 712–719.
[28] X. Hu, R. Barker, A. Neville, A. Gnanavelu, Case study on erosion–corrosion degradation of pipework located on an offshore oil and gas facility, Wear 271 (2011) 1295–1301.
[29] X. Hu, A. Neville, CO_2 erosion–corrosion of pipeline steel (API X65) in oil and gas conditions—a systematic approach, Wear (2009), http://dx.doi.org/10:1016/j.wear.2009.07.023. (accessed on 02.12.2010).
[30] D.C. Silverman, Rotating cylinder electrode for velocity sensitivity testing, Corrosion (1984) 20.
[31] D.C. Silverman, Rotating cylinder electrode—geometry relationships for prediction of velocity-sensitive corrosion, Corrosion 44 (1) (1987) 42.
[32] X. Jiang, Y.G. Zheng, W. Ke, Effect of flow velocity and entrained sand on inhibitor performances of two inhibitors for CO_2 corrosion of N80 steel in 3% NaCl solution, Corrosion Science 47 (2005) 2636–2658.
[33] L.P. Hammet, Physical Organic Chemistry, 32, McGraw-Hill Book Co., Inc., New Yorkpp. 965–997, Chapters III, IV, V.
[34] M. Mörtsell and M. Gullikkson, An overview of some non-linear technique in chemotrics, 2001, miun-diva-portal.org/smash/get/diva2:227164/FULLTEXT01, (accessed on 24.01.2013).
[35] I. Finnie, Some reflections on the past and future of erosion, Wear 186–187 (Part 1) (1995) 1–10.
[36] J.F. Flores, A. Neville, N. Kapur, A. Gnanavelu, Erosion–corrosion degradation mechanisms of Fe–Cr–C and WC–Fe–Cr–C PTA overlay in concentrated slurries, Wear 267 (II) (2009) 1811–1820.
[37] S. Nesic, Key issues related to modeling of internal corrosion of oil and gas pipelines—a review, Corrosion Science 49 (2007) 4308–4338.
[38] H.M. Shalaby, S. Attari, W.T. Riad, V.K. Gouda, Erosion corrosion behavior of some cast alloys in seawater, Corrosion 48 (1992) 206–217.
[39] B.R. Linter, G.T. Burstein, Reactions of pipeline steels in CO_2 solutions, Corrosion Science 41 (1) (1999) 117–139.
[40] S. Nesic, G.T. Solvi, J. Enerhaug, Comparison of the rotating cylinder and pipe flow test for flow-sensitive CO_2 corrosion, Corrosion 51 (10) (1995) 773–787.
[41] D.M. Ortega-Toledo, J.G. Gonzalez-Rodriguez, Casales, A. Cacares, L. Martinez, Hydrodynamic effects on the CO_2 corrosion inhibition of X-120 pipeline steel by a modified imidazoline under flow conditions, Corrosion Science 53 (2011) 3780–3787.
[42] E.E. Oguzie, Corrosion inhibition of Aluminum in acidic and alkaline media bysansevieria trifasciata extract, Corrosion Science, 49 1527–1539.
[43] Branzoi V., Branzoi F., Baibarac M.M., The inhibition of the corrosion of Armco iron in HCl solutions in the presence of surfactants of the type of N-Alky; quaternary ammonium salts, Mater. Chem. Phys. 65 (2000) 288–297.
[44] Wang, Erosion–corrosion of engineering steels—can it be managed by use of chemicals? Wear 267 (2009) 2018–2026.
[45] X. Fan, W. Liu, F. Cai, H. Guo, Y. Wu, Q. Du, M. Lu, Electrochemical Characterization of Erosion–Corrosion of X70 Pipeline Steel under Jet Impingement Conditions, NACE International, Houston, TX, 2011. (CORROSION/2011, Paper no. 11241).
[46] X. Hu, K. Alzawai, A. Gnanavelu, A. Neville, C. Wang, A. Crossland, J. Martin, Assessing the effect of corrosion inhibitor on erosion–corrosion of API-5L-X65 in multi-phase jet impingement conditions, Wear 271 (2011) 1432–1437.